

# Interfacial Solar Steam Generation Enabled by A Blackest Absorber

XIAOJIE LIU,<sup>1</sup> YANPEI TIAN,<sup>1</sup> FANGQI CHEN,<sup>1</sup> RALPH AHLGREN,<sup>2</sup>  
YITING ZHENG,<sup>3</sup> MING SU,<sup>3</sup> GANG XIAO,<sup>4</sup> AND YI ZHENG,<sup>1,\*</sup>

<sup>1</sup>*Department of Mechanical and Industrial Engineering, Northeastern University, Boston, MA 02115, USA*

<sup>2</sup>*Soleeva Energy, Inc. San Jose, CA 95131, USA*

<sup>3</sup>*Department of Chemical Engineering, Northeastern University, Boston, MA 02115, USA*

<sup>4</sup>*Department of Physics, Brown University, Providence, Rhode Island 02912, USA*

\**opex@osa.org*

**Abstract:** Solar-driven interfacial steam generation for desalination has attracted broad attention. However, a significant challenge still exists for achieving a fast evaporation rate and high quality of water together with the low-cost and simple-to-manufacture device to provide a feasible solar-driven steam generation system. In this study, a novel "blackest" paint Black 3.0 serving as a perfect solar absorber is introduced into the hot-pressed melamine foam (MF) networks, constructing the blackest (99% absorptance in the solar region) and self-floating evaporation device. The features of effective solar absorptance and salt-rejection capability contribute to a high evaporation rate at  $2.48 \text{ kg m}^{-2} \text{ h}^{-1}$  under one sun ( $1 \text{ kW m}^{-2}$ ). This interfacial solar evaporator has a daily clean water yield of  $2.8 \text{ kg m}^{-2}$  even in cloudy winter weather and keeps stability in wide degrees of acidity and alkalinity (pH 1~14) water. This feature shines remarkable lights on a facilely fabricated, robust, high-efficient, and cost-effective solar steam generation system.

© 2022 Optical Society of America under the terms of the [OSA Open Access Publishing Agreement](#)

## 1. Introduction

Access to freshwater is of pivotal importance to humans. However, the high rate of population growth and climate change presents an increased need for fresh water, and water scarcity has become a treat to the sustainable development of human society [1, 2]. This motivates the development of utilizing saline waters from the oceans and other brackish water sources and the processes that convert saltwater into freshwater. Solar energy is now emerging as one of the most promising sustainable energy sources, and it's the greatest advantage is clean and can be supplied without any environmental pollution compared with other forms of energy [3]. And abundant solar energy makes the solar-driven evaporation one of the promising approach for desalination. In a conventional bulk heating solar-driven evaporation system, bulk water is heated to a high temperature to generate water vapor, which results in a slow response to sunlight and heat loss to bulk water or the external environment [4–8]. In 2011, Wang et al. were one of the first demonstrating the floating interfacial solar-driven evaporation structure into desalination area, which does not require high-cost permanent construction or land use, and capital investment [9]. Compared with bulk water-heating method which heats the entire body of water, the interfacial solar-driven evaporation approach mainly localizes the heat generation the water-air interface, avoids heating an entire large volume of water, especially for the ocean, which regards as a low-temperature sink, and lead to the ultra-fast response to the sunlight and higher systematic thermal efficiency [10, 11]. Furthermore, the interfacial solar-driven evaporation can be easily applied by floating the absorber sheet on the water surface without complex pressure control and other complex infrastructure. Owing to all of these advantages mentioned above, scientists have made great efforts to exploit, develop, and optimize the interfacial solar-driven evaporation.

To yield remarkable photothermal performance, the development of interfacial evaporation

structure should center around the following three key factors: (1) The ideal solar absorber should possess outstanding absorbance in the range of visible and near-infrared region [12] and then convert these solar radiation energies into heat which used to generate the water vapor; (2) It is crucial for the interfacial evaporation to own the low thermal conductivity characteristic to localize the heat at the air/water evaporative interface and reduce heat loss from the absorber to the low-temperature bulk water; (3) High hydrophilicity and porous framework are necessary for the sufficient water transport from the bulk water to heated area; and (4) Self-floating ability is another one of important factors for the evaporation system, which avoid using permanent construction or land use, and can be placed directly on the water surface. More and more researchers gravitate towards the interfacial solar-driven evaporation by its efficient evaporative performance and tried to find a kind of material or structure to match these key factors mentioned above, however, it is still a challenge find a one-component material that can satisfy all of these critical factors. To obtain the extremely high-energy efficiency, a multilayered interfacial evaporation structure was proposed which fits well these pivotal factors and provides us more options to choose different appropriate corresponding material [13–17]. Ghasemi et al. first demonstrated the double-layered structure consisting of a carbon foam layer supporting an exfoliated graphite layer [15]. The bottom layer serves as a heat barrier to minimize the heat loss to the bulk water, and its porous structure used to transport water from nether water to the heated area, and at the same time, it can support the top layer which fulfills the self-floating demand. The top layer plays the part of the absorber to receive the solar energy, and its porous structure is for the vapor leaving. After that, many similar double-layered evaporation structures were widely adopted. In most of previous work focusing on the double-layered evaporation structure, bottom layer usually integrate the water transport channel and heat barrier into one entity, like air-laid paper [18], polystyrene foam [13], woodblock [19–21], polyurethane sponge [22], macroporous silica substrate [23], bacterial nanocellulose aerogel [24]. However, at steady working condition, when a bountiful supply of water transported to the top photothermal area via the bottom layer, almost all of the macropores of heat barrier were filled with water, whose heat conductivity is generally higher than that of the heat barrier materials, weakening the effect of the heat barrier. To avoid losing heat through a porous heat barrier in the double-layered structure, in a recent study, a new multilayered evaporation structure consisting of photothermal material, closed-pore thermal insulator, and external hydrophilic materials has been of major interest. The closed-pore thermal insulator serves as the real heat barrier layer and the air inside the insulator plays an important role in reducing heat conduction. For example, polystyrene foam [16, 17, 25–28] is a good choice for the thermal insulator in consideration of its low thermal conductivity and its low cost. External hydrophilic materials, wrapping or passing through the insulator foam, act as a capillary-driven pump with a 1D/2D water path [17, 29]. By and large, this modified multilayered evaporation structure has become a favorable way to further minimize heat conduction losses and improve energy conversion efficiency. The efficient solar steam generation highly depends on the photothermal conversion materials with broadband absorbance and high photothermal properties [30, 31]. On the basis of multilayered structure, diverse photothermal materials with wide light absorbance have been extensively studied, including carbon-based materials [9, 15, 32, 33], metal [34–37], and metal oxides [38–41]. Carbon-based absorbers, such as carbon black [42], graphene [43], graphene oxide [17, 24, 44] and carbon nanotube [21, 23], offer great advantages of high solar absorbance and stability, and they have become the largely approving choices, however, the utilization of elaborate technologies and high associated cost limit their field application on large-scale desalination to a certain extent [6, 17, 45]. Although metal-based materials have attracted tremendous attention in the solar-driven evaporation direction because of their unique optical and photothermal properties, like Au NPs [18, 46, 47], their chemical and thermal stability, exorbitant cost, complicated processing processes, and high requirement of specialized fabrication are obstacles for future industrial application. Therefore, it is inescapable to explore

the novel techniques and materials to increase the evaporation efficiency and decrease the cost of desalination.

In this work, a novel commercial paint Black 3.0, the blackest black paint, was first applied to the floating interfacial solar-driven evaporation device serving as the photothermal conversion material combined with a sheet of MF. Herein, a sheet of hot-pressed MF played the ideal elastic skeleton material sprayed with Black 3.0 serving as a solar absorber to efficiently absorb and convert the solar radiation into heat. To realize high evaporation performance and high solar-thermal energy conversion efficiency, we demonstrate a self-floating three-layer evaporation structure with a 2D water path to localize solar-thermal heat generation to the interface. This device made from commercially available materials: solar absorber is a sheet of hot-pressed MF combined with Black 3.0 paint; 2D water path provided by Webril all-cotton wipes with highly absorbent, and thermal barrier is Polyvinyl chloride (PVC) foam. Under 1 sun solar illumination without solar concentration, the evaporation device showed an excellent evaporation rate as high as  $2.48 \text{ kg m}^{-2} \text{ h}^{-1}$  and a highlighted evaporation efficiency of 172.5%. Based on the multilayered evaporation structure, the novel commercial paint Black 3.0 demonstrates a superb performance with cost-effectiveness, operability, and durability, which can be regarded as one of the indispensable choices of the solar-absorbing materials in the development of solar-driven evaporation process.

## 2. Experimental section

### 2.1. Materials

The commercial MF sold by South Street Designs company (UPC: 089902974060) with the dimension of  $10 \text{ cm} \times 6 \text{ cm} \times 2 \text{ cm}$  (\$0.3/piece). Black 3.0 paint was purchased on the Culture Hustle official website (\$0.146/mL). Webril pure cotton wipe is in the size of  $0.2 \text{ m} \times 0.2 \text{ m}$  (\$2.99/m<sup>2</sup>). The PVC foam insulator sheet was purchased from the McMaster-Carr with the dimension of  $81 \text{ cm} \times 81 \text{ cm} \times 1.9 \text{ cm}$  (\$76.03/sheet).

### 2.2. Sample preparation

Solar absorber layer was fabricated as follows: pristine MF as we received was thoroughly washed several times with ethanol and deionized (DI) water and then put in the oven keeping at  $60 \text{ }^\circ\text{C}$  in preparation for hot-pressing treatment. After it was totally dried, the MF was pressed at  $200 \text{ }^\circ\text{C}$  for 6 min with the compression ratio of 4, which is the height ratio of pristine MF to hot-pressed MF. Serving as the skeleton of the absorber, hot-pressed MF was cut into the desired shape with a thickness of about 1 mm. Black 3.0 paint was thinned with DI water under vigorous stirring for 5 min with a paintbrush, which helps a lot to get a homogeneous mixture. The mass ratio of DI water to Black 3.0 was kept in the range of 0.35~0.4 in the dilution process. Subsequently, the diluted Black 3.0 paint was sprayed onto the MF sheet by a touch-up spray gun (Paasche Airbrush, USA) with a 0.8 mm spray head at the pressure of 70 psi. The distance between the spray head and the MF sheet was about 25 cm. The golden rule is that 3 or 4 thin layers is much better than a big thick layer. And then dried it between sprays with the hot air blower (Yihua Electronic Equipment Co., Ltd, Guangzhou, China) at a temperature of  $190 \text{ }^\circ\text{C}$  for 5 min. It's worth noting that this drying time is suitable for the dimension of the sample in this work.

A piece of PVC foam (47 mm in diameter and 19 mm in thickness) was utilized as the thermal insulator. Webril pure cotton wipe was cut into a 47 cm circle having four extended strips with 30 mm in width and 19 mm in length. The hydrophilic cotton wipe was wrapped around the PVC foam letting the four strips tip soak in the bulk water to ensure that the water could reach the upper circle area by capillary force. Then, the MF sheet was placed over the circle area of the cotton wipe. The whole cost for this evaporation device is around 0.58 dollars.

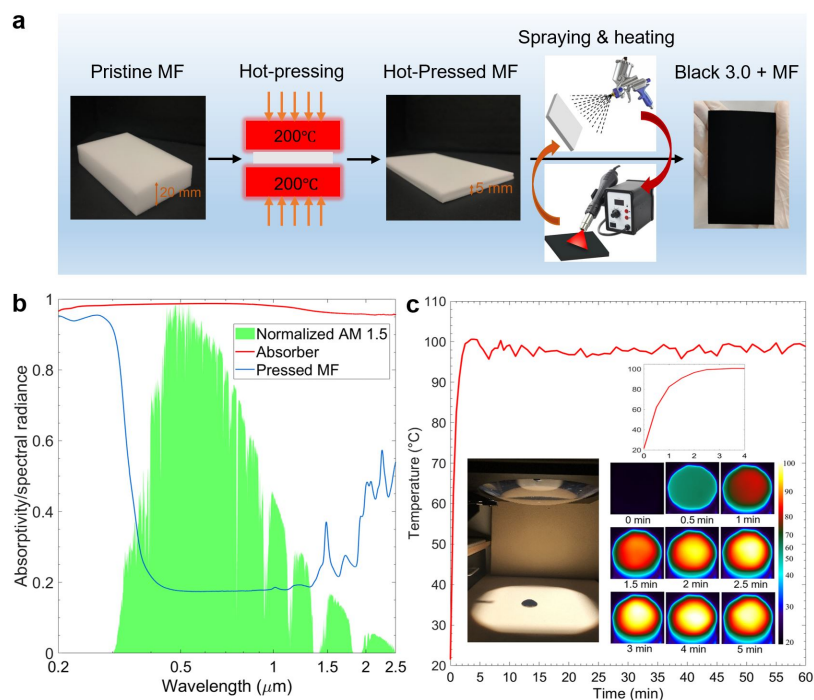


Fig. 1. Preparation process and characterizations of the absorber layer. (a) Schematic illustration of the fabrication of the absorber layer in the evaporation device. (b) UV-Vis-NIR absorption spectra of the absorber layer, pressed MF, and the normalized spectral solar irradiance density of air mass 1.5 global (AM 1.5 G) tilt solar spectrum. (c) The temperature changes of the absorber sheet overtime under 1 sun.

### 2.3. Solar steam generation experiments

The steam generation experiments in the lab were carried out under a solar simulator (Newport, 94081A, class ABB) which supplying solar flux of  $1 \text{ kW m}^{-2}$  with an optical filter for the standard AM 1.5 G spectrum. 127 g of DI water and seawater (3.5 wt% NaCl) were prepared with the same initial temperature of  $21 \text{ }^\circ\text{C}$  and placed in the 100 mL beakers with a mouth diameter of 50 mm. The steam generation device was floated on the solution surface and the mass change of water was accurately monitored by an electric balance (RADWAG, PS 1000.X2.NTEP) connected to a computer for recording the real-time mass value. The real-time temperature was monitored by an infrared radiation camera (FLIR, A655sc).

## 3. Results and discussions

The schematic of the synthesis process of the absorber layer is shown in Fig. 1a. The fabrication process is simple and scalable, which was summarized as three steps: hot-pressing, spraying and drying. In this study, the MF with the dimension of  $10 \text{ cm} \times 6 \text{ cm} \times 2 \text{ cm}$  was selected as an elastic skeleton for immobilization of Black 3.0 spray. MF is a commercially available low-cost polymer material, and it's high porosity, low density, excellent hydrophilicity, and elasticity making it highly used for the solar steam generation device [45, 48]. Considering the absorber layer is about 1 mm in thickness, hot-pressing treatment of the MF is helpful to increase its elasticity and fatigue resistance, more importantly, the compressed 3D network of the foam can dramatically increase its density to effectively increase the light area in such thickness. Pristine MF with a thickness of 20 mm was pressed at  $200 \text{ }^\circ\text{C}$  for 6 minutes, and the thickness of the

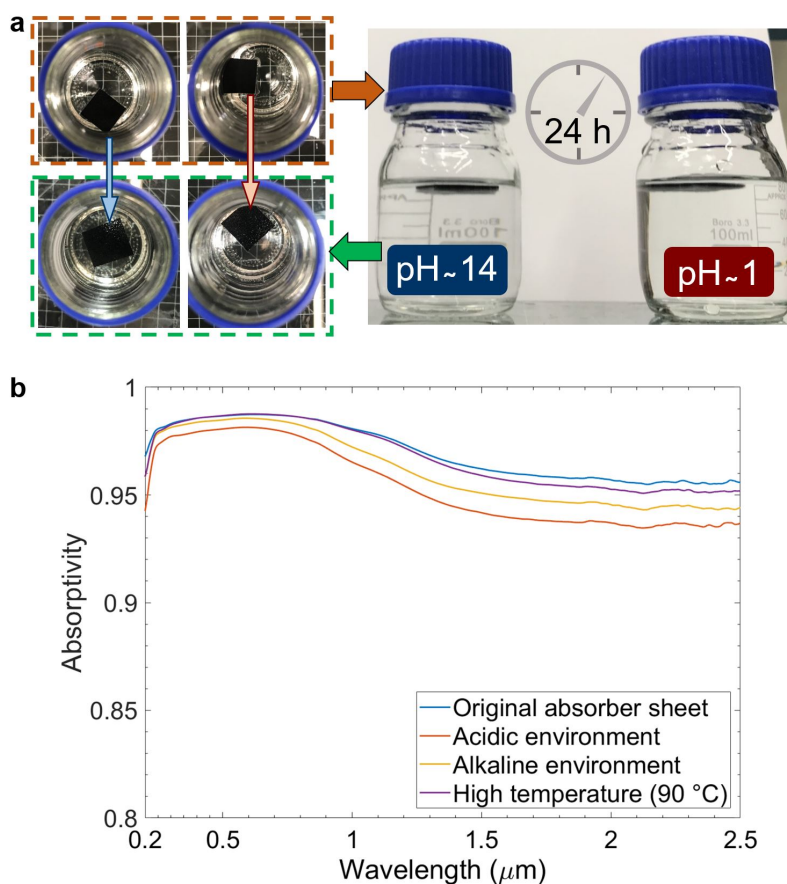


Fig. 2. The stability of the absorber layer test under different harsh environment. (a) The absorber layer was immersed in alkaline solution (PH ~14) and acidic solution (PH ~1) for 24 hours in the closed bottles. (b) UV-Vis-NIR absorption spectra of absorber layer in different harsh environment.

hot-pressed MF was kept at 5 mm. Then, the pressed MF was cut into the desired shape with about 1 mm in thickness. For our laboratory experiments, the pressed MF was cut into a circle of 47 mm in diameter corresponding to the size of the beaker in 100 ml. As the blackest acrylic paint, Black 3.0 has gained great attention in creative art, and now, it would be a rising star of solar photothermal material mainly because (1) As the blackest and most matte acrylic paint on the planet, Black 3.0 exhibits nearly perfect solar absorption, which absorbs up to 99% of visible light; (2) It's super easy to brush or spray it on most surfaces, like wood, paper, canvas, and plastic; (3) It's lightfast character can not be ignored when it was applied to desalination process; (4) its straightforward and simple operating instructions and affordable price make it widespread. Then the diluted paint was added into the spray gun and sprayed on the pressed MF sheet (47 mm in diameter). The distance between the spray head and the MF sheet was about 25 cm. Because of the porous surface of the pressed MF sheet surface, a couple of thin coats is better than one big thick one. During each coat, drying it thoroughly with hot air at 190 °C for 5 minutes. After last utterly drying, the Black 3.0-coated MF sheet was rinsed in DI water for several times to remove the residual impurities. Hereafter, keeping this sheet in the oven at 60 °C to dry to serve as the solar absorber layer in the evaporation device. The absorber layer

was successfully manufactured without any expensive equipment or complex process which is extremely suitable for scalable preparation. As shown in Fig. 1b, the absorber sheet exhibits a superb absorption ranging from 95% to 99% at the wavelength of 0.2  $\mu\text{m}$  to 2.5  $\mu\text{m}$ , indicating that it acts as an efficient broadband solar radiation absorber, whereas the pure pressed MF shows only poor absorption. To evaluate the stability of the absorber sheet, the absorber layers underwent severe tests, kept in the boiling water (around 90  $^{\circ}\text{C}$ ) for 2 hours and immersed in the alkaline solution (PH  $\sim$ 14) and acidic solution (PH  $\sim$ 1) for 24 hours in the closed bottles. After this harsh test, no obvious changes in the appearance and their absorption spectrums basically consistent with the previous one (Figure support). Fig. 1c shows the surface temperature of the absorber sheet in the air under one 1 sun for an hour. The time-dependent temperature changes and images were captured by an infrared camera at room temperature, displaying the maximum temperature of the sheet versus time curves. In taking the temperature measurement, the tested sample was placed on the PVC foam plate to minimize the heat exchange with the base below. Upon light illumination, the surface temperature of the absorber sheet rose sharply to an equilibrium temperature around 100  $^{\circ}\text{C}$  within the initial 2.5 minutes and then floated slightly around this temperature afterward, indicating the excellent photothermal performance of the absorber sheet. The insert figure demonstrated the changes in surface temperature more clearly in the initial 4 minutes.

Localizing the heat converted from solar energy to the air/water interface is the critical step to achieve high evaporation performance. Fig. 3a demonstrated the self-floating evaporation device structure which is composed of three layers. The top layer is a solar absorber layer of the MF sheet combined with Black 3.0 and it played an essential role in the efficient absorption of the solar radiation. Beneath the absorber layer is a 2D water path that is enabled by a cotton wipe cut into the shape of a circle with 4 extended strips. The round area of the cotton wipe was kept inconsistent with the absorber area, and the bottom side of 4 strips was in direct contact with the bulk water, which decreased the contact area between the evaporation surface and the bulk water. The cotton wipe was used to transport water via its strong capillary force and to reduce the direct contact between the bulk water and the absorber layer. Simultaneously ensuring the efficient water supply to the solar heating area and minimizing the heat dissipation to the bulk water is crucial to high-efficiency interfacial evaporation. The interlocked fibers of cotton wipe won't come apart when soaked in water for a long time which contributes to the durability and stability of the evaporation device. In the working process, the cotton wipe pumped the bulk water towards the heating surface through the 4 strips around the floating foam relying on its strong capillary wicking effect. The bottom layer is the thermal insulation wrapped with the cotton water path. The thermal insulation is made from PVC foam with only closed pores which are impermeable to water, and its low thermal conductivity ( $\sim$ 0.03  $\text{W m}^{-1} \text{K}^{-1}$ ) almost reduced the downward thermal dissipation from the evaporation surface. Thanks to the low density of the thermal insulation and the simple structure of the whole device, the evaporation device can be placed on the water and move together with the waving water surface achieving self-floating for continuous operation.

The surface wettability of the evaporation device also played an important role in the steam generation process. As shown in Fig. 3b, the evaporation device with a diameter of 47 mm was placed in a beaker filled with DI water at the initial temperature of 21  $^{\circ}\text{C}$ , and its wetting process was recorded on the top view. It is obvious that the water immediately reached the surface of the absorber layer from the regional edge (the area in the blue dashed curve), and then the wet area quickly expanded to the central area until it covered the entire evaporation surface. The surface wettability owes much to forceful hydrophilicity of the cotton 2D water path and the porous structure of the absorber layer, which assure ample water supply to the evaporation surface.

Avoiding salt accumulating in the evaporation device remains a significant character for the self-floating solar evaporation structure utilizing heat localization [16]. Fig. 3c shows the

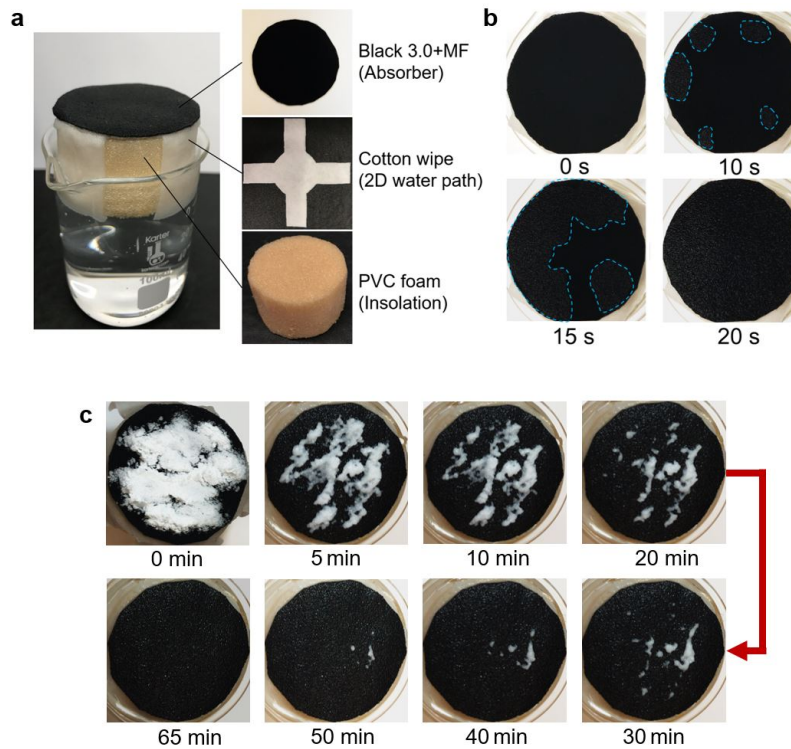


Fig. 3. The self-floating evaporation device with surface wettability and salt rejection ability. (a) Photographs of three-layer evaporation device placed in the beaker filled with water. (b) Wetting process of the evaporation device when place it on the surface of water. The area inside the blue dashed curves exhibits the wet parts. (c) salt rejection progress of the evaporation device. The evaporation device was placed in a beaker filled with 3.5 wt% NaCl solution, and NaCl is stacked on the absorber surface.

progression of salt dissolution which demonstrated the salt rejection ability of the three-layer device. In this experiment, a three-layer structure device with a diameter of 47 mm floated in a 100 ml beaker of 132 g 3.5 wt% NaCl solution with 21 °C initial temperature, and 1.7 g of additional solid NaCl was placed directly on the device. Upon contact with water, the solid NaCl started to dissolve due to the movement and exchange of solution inside the absorber layer and 2D water path between the device surface and the bulk water below the insulation. After approximately 65 minutes, the three-layer device fully rejected the salt, indicating its salt rejection ability.

The steam generation ability of the evaporation device at laboratory scale was tested combining an irradiation system to simulate the solar radiation, a weighing system to monitor the mass change of water in the beaker during certain time irradiation, and an infrared monitoring system to monitor the real-time temperature, as shown in Fig. SX. In the laboratory test experiments, the diameter and thickness of the evaporation device are 47 mm and 19 mm, respectively. Both 3.5 wt% NaCl solution and DI water were prepared to keep the initial temperature at 21 °C in the 100 ml beaker. The evaporation device floated on water in the beaker filled with 127 g of water, beneath the beaker is an electronic balance connected to the computer, and the simulated solar radiation was provided by a solar simulator. When the illumination began, the solar steam generation was determined by the balance, and the real-time temperature of the absorber sheet and water surface were monitored by the IR camera. The laboratory temperature and humidity

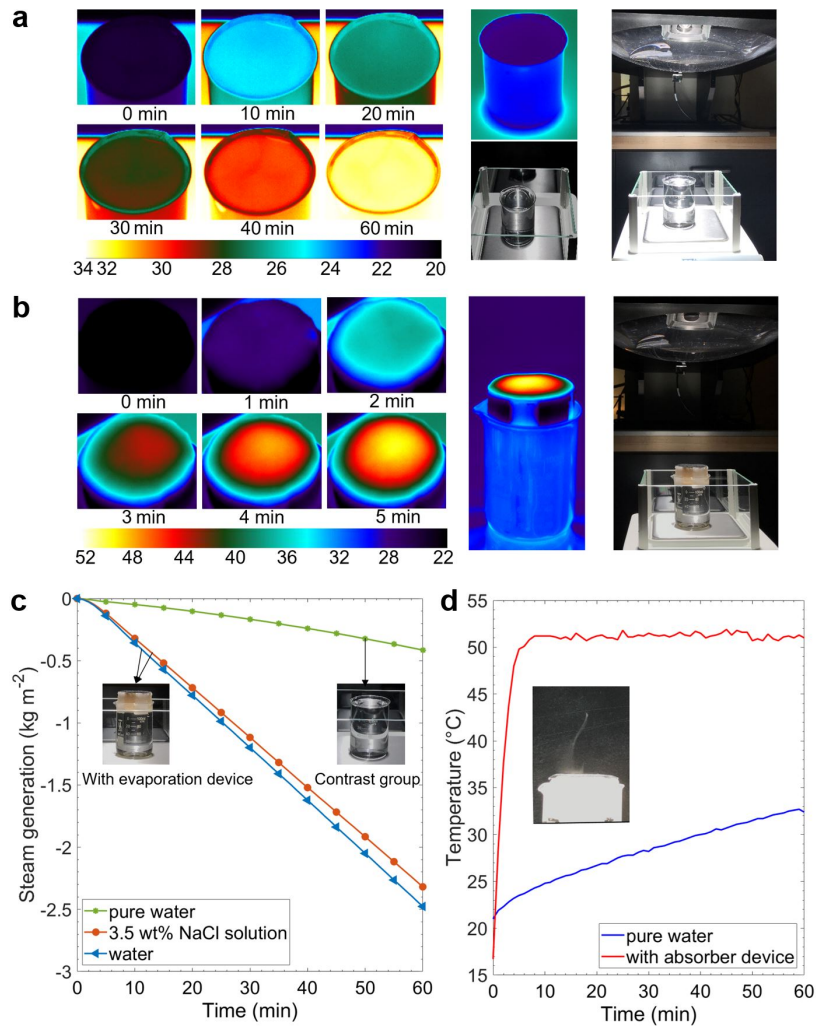


Fig. 4. (a) Left: IR thermal images of top surface of water-only beaker under 1 sun illumination over irradiation time. Middle: IR thermal image and the photograph of the beaker filled with DI water only under 1 sun after one hour. Right: The photograph of the beaker filled with water only placed on an electrical balance under 1 sun illumination. (b) Left: IR thermal images of evaporation device on the top view under 1 sun illumination in the initial 5 minutes. Middle: IR thermal image of the evaporation device floated on water in the beaker under 1 sun illumination after one hour. Right: The photograph of the beaker with the evaporation device placed on an electrical balance under 1 sun illumination. (c) The mass changes of water versus time of DI water only, evaporation device in DI water and 3.5 wt% NaCl solution. (d) The maximum temperature profiles of the pure water surface and the absorber layer under 1 sun illumination over irradiation time. The inset is the visible steam flow generated under 1 sun irradiation.

were kept at about  $22^{\circ}\text{C}$  and 21%, respectively.

Figure 4 compares the surface temperatures of pure water and with evaporation device under 1 sun illumination. The temperature data and images were captured by the IR camera. Fig. 4a showed the surface temperature distribution of the beaker without the evaporation device over the

irradiation time. The surface temperature raised slowly under irradiation owing to the poor light harvest efficiency and its maximum temperature profile shown in Fig. 4d sloped gently from the initial temperature of 21 °C to the 32 °C for an hour. In contrast, upon light illumination, the temperature of the absorber layer rose sharply to an equilibrium temperature around 50 °C, indicating good photothermal performance As shown in Fig. 4c, for the water only experiment, the steam generation rate is measured to be 0.41 kg m<sup>-2</sup> h<sup>-1</sup> Under 1 sun irradiation (1 kW m<sup>-2</sup>). In contrast, the steam generation rate of evaporation device in DI water reached up to 2.48 kg m<sup>-2</sup> h<sup>-1</sup> under the same experimental conditions, corresponding to 6.04 times higher than that of water only case. Significantly, when the evaporation device floated on 3.5 wt% NaCl solution, it exhibited the comparable steam generation rate of 2.32 kg m<sup>-2</sup> h<sup>-1</sup> which is 5.65 times higher than that of water only case at the same experimental conditions. Evaporation efficiency,  $\eta_{evap}$ , is an important figure to evaluate the steam generation performance and it can be calculated by the equation of  $\eta_{evap} = \dot{m}h_{fg}/Q_s$ . where  $\dot{m}$  is the water evaporation rate (kg m<sup>-2</sup> h<sup>-1</sup>),  $Q_s$  is the power density of incoming light illumination (kW m<sup>-2</sup>), and  $h_{fg}$  is the total enthalpy of vaporization of water (kJ kg<sup>-1</sup>). In particular,  $h_{fg}$  was regarded as the sum of sensible heat (121.26 kJ kg<sup>-1</sup>) and temperature-dependent enthalpy of vaporization (2382.7 kJ kg<sup>-1</sup>) in this text. Therefore, the corresponding value of evaporation efficiency is 172.5% under one sun illumination.

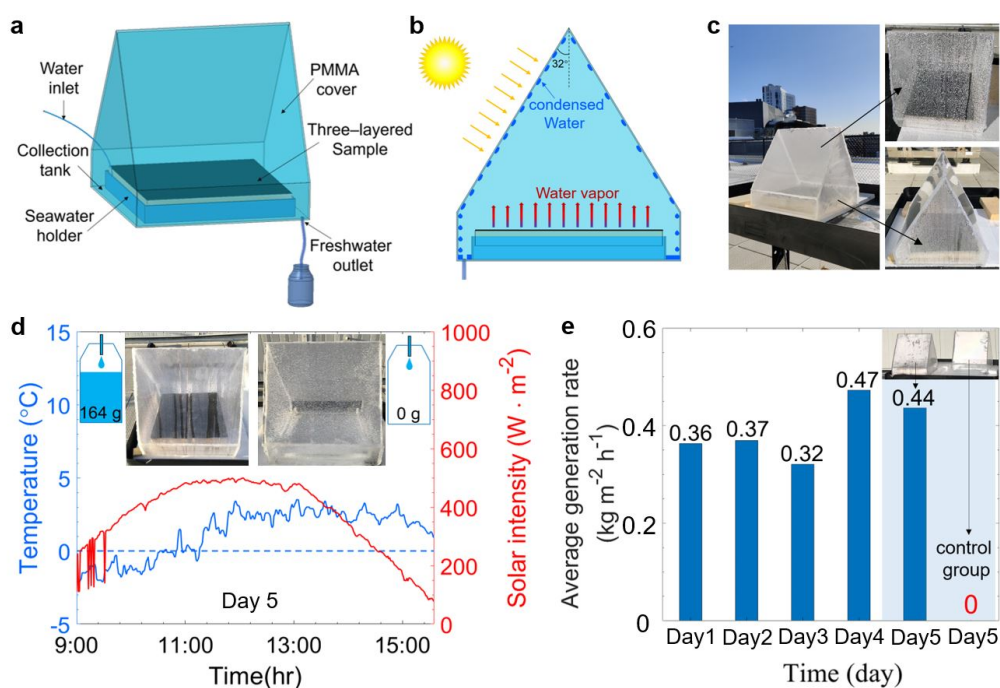


Fig. 5. Rooftop experiments with evaporation system under natural sunlight in January. (a) 3D model of the evaporation system with condensation cover in the dimension of 30 cm × 30 cm for desalination. (b) Schematic illustration of desalination solar still. (c) Photograph of evaporation system placed on the cart (left) and dense condensed water droplets on the condensation cover and sidewall (right) during the experiment time. (d) The contrast experiment with evaporation device (left inset) and without (right inset) on day 5. The blue curve and red curve showed the various temperature of ambient and solar intensity, respectively. Two bottles showed the weight of the collected water. (e) Average hourly steam generation rate in 5 days.

#### 4. Field test

This evaporation device was also future verified that the scalable production of freshwater is possible with this set-up, a prototype of evaporation system with condensation chamber and evaporation device of a larger area of the absorber (24 cm × 24 cm) inside was constructed. The composition and design of the prototype are shown in Figs. 5a and SX. The condensation chamber made of Polymethyl methacrylate (PMMA) board was developed to surround the evaporation device to capture and condense the solar-evaporated steam. According to the transmission spectrum of the PMMA board, shown in Fig. SX, the condensation structure is transparent in the solar spectrum to allow the solar irradiance to reach the evaporation device, while it is opaque in the mid-infrared region to confine the infrared emission of the evaporation device inside the chamber to contribute to maintaining a relatively higher evaporation temperature. As shown in Fig. 5b, the tilted angle of the condensation cover in the dimension of 30 cm × 30 cm is fixed to be 32°, allowing the solar flux reaches the evaporator without refraction. In Fig. 5c, this photograph showed the prototype was placed on the 2mm thick polystyrene foam, which with a low thermal conductivity to reduce the thermal flux between the bottom of the prototype and the cart, and the condensed water was observed on the condensation cover (Fig. SX). The condensed water droplets will fall to the collection tank and eventually flow to a chemical storage bottle. The salinities ( $\text{Na}^+$ ) of desalinated water () is much lower than the standard specified by the World Health Organization (WHO) [49]. The validated prototype was tested on the roof of Northeastern University, Boston, USA, and water collections were measured over 5 days during the winter. The specific experiment date, instantaneous incident sunlight, ambient temperature, wind speed, and humidity were recorded. The 3.5wt% NaCl solution, which simulates the average salinity of seawater across the world ocean, was used during the test and the seawater holder was filled up through the water injection tube after each day use.

The average hourly output rate, shown in Fig. 5e, varied from 0.32 to 0.47  $\text{Kg m}^{-2} \text{h}^{-2}$  under various solar intensity and ambient temperature. The experiment data and detailed weather condition data were provided in Figs. SX and SX. To exhibit the promising solar steam generation ability of this evaporation system, the prototype, and the control group, having the same condensation chamber without a three-layer evaporation device inside was conducted contrast experiments on day 5 (Fig. 5d). At the end of the experiment, 164 g of water was collected from the prototype, while the control group collected none water during the same-day operation. In the rooftop experiments, the weight of collected freshwater in the text refers to the weight of water in the chemical storage bottle, not exactly the weight of condensed water produced. The inset of Fig. 5d shows the end state of the contrast experiment. Obviously, in the control group, dense condensed water droplets can be observed on the cover without forming water flow (Fig. SX). In day 4, the daily condensate rate ( $2.83 \text{ kg m}^{-2} \text{ d}^{-1}$ ) in winter produced from our  $0.0576 \text{ m}^{-2}$  evaporation is comparable to a previous work ( $2.81 \text{ kg m}^{-2} \text{ d}^{-1}$ ) in the summer [16], which proves the scalable production of our design.

#### 5. Conclusions

In summary, we have demonstrated a high-performance and cost-efficient fabrication of interfacial three-layer steam generation devices based on the novel commercial paint Black 3.0 which was first applied to the solar steam generation as a promising candidate for the photothermal materials. Black 3.0 sprayed on a sheet of MF served as the top solar absorber layer that can widely absorb the solar radiation and efficiently convert it into heat. The absorber layer placed on a PVC foam plane under 1 sun irradiation showed a significant temperature gradient and reached up to 100 °C of equilibrium temperature. It also exhibited strong stability under various extremely harsh environment and remarkable salt rejection ability, both of these performances contributed to the long-term durable steam generation process. In the laboratory experiments, enabled by the

assist of PVC foam to reduce the heat loss and the cotton wipe to provide sufficient water to the heating region, the evaporation device has reached a striking steam generation rate of  $2.48 \text{ kg m}^{-2} \text{ h}^{-1}$ , 6 times higher than the natural evaporation, and a highlighted evaporation efficiency of 172.5% under 1 sun irradiation in the room temperature, surpassing most of the reported works. Even in the rooftop experiments for a cloudy Boston winter day with the maximum environment temperature of  $4 \text{ }^\circ\text{C}$ ,  $2.83 \text{ kg m}^{-2} \text{ d}^{-1}$  of water was collected. Moreover, this evaporation device with low-cost in the aspect of both materials and fabrication, coupled with its super simple preparation, made it has significant practical applications on large-scale.

### **Acknowledgements**

This project is supported partly by the Soleeva Energy Innovation Award and the National Science Foundation through grant numbers CBET-1941743.

## References

1. M. M. Mekonnen and A. Y. Hoekstra, "Four billion people facing severe water scarcity," *Sci. advances* **2**, e1500323 (2016).
2. J. H. Reif and W. Alhalabi, "Solar-thermal powered desalination: Its significant challenges and potential," *Renew. Sustain. Energy Rev.* **48**, 152–165 (2015).
3. S. A. Kalogirou, "Solar thermal collectors and applications," *Prog. energy combustion science* **30**, 231–295 (2004).
4. A. Kabeel and S. El-Agouz, "Review of researches and developments on solar stills," *Desalination* **276**, 1–12 (2011).
5. O. Neumann, A. S. Urban, J. Day, S. Lal, P. Nordlander, and N. J. Halas, "Solar vapor generation enabled by nanoparticles," *ACS nano* **7**, 42–49 (2012).
6. P. Tao, G. Ni, C. Song, W. Shang, J. Wu, J. Zhu, G. Chen, and T. Deng, "Solar-driven interfacial evaporation," *Nat. energy* **3**, 1031–1041 (2018).
7. A. Lenert and E. N. Wang, "Optimization of nanofluid volumetric receivers for solar thermal energy conversion," *Sol. Energy* **86**, 253–265 (2012).
8. N. J. Hogan, A. S. Urban, C. Ayala-Orozco, A. Pimpinelli, P. Nordlander, and N. J. Halas, "Nanoparticles heat through light localization," *Nano letters* **14**, 4640–4645 (2014).
9. Y. Zeng, J. Yao, B. A. Horri, K. Wang, Y. Wu, D. Li, and H. Wang, "Solar evaporation enhancement using floating light-absorbing magnetic particles," *Energy & Environ. Sci.* **4**, 4074–4078 (2011).
10. P. Wang, "Emerging investigator series: the rise of nano-enabled photothermal materials for water evaporation and clean water production by sunlight," *Environ. Sci. Nano* **5**, 1078–1089 (2018).
11. Z. Wang, Y. Liu, P. Tao, Q. Shen, N. Yi, F. Zhang, Q. Liu, C. Song, D. Zhang, W. Shang *et al.*, "Bio-inspired evaporation through plasmonic film of nanoparticles at the air–water interface," *Small* **10**, 3234–3239 (2014).
12. P. Zhang, J. Li, L. Lv, Y. Zhao, and L. Qu, "Vertically aligned graphene sheets membrane for highly efficient solar thermal generation of clean water," *Acs Nano* **11**, 5087–5093 (2017).
13. L. Shi, Y. Wang, L. Zhang, and P. Wang, "Rational design of a bi-layered reduced graphene oxide film on polystyrene foam for solar-driven interfacial water evaporation," *J. Mater. Chem. A* **5**, 16212–16219 (2017).
14. J. Lou, Y. Liu, Z. Wang, D. Zhao, C. Song, J. Wu, N. Dasgupta, W. Zhang, D. Zhang, P. Tao *et al.*, "Bioinspired multifunctional paper-based rgo composites for solar-driven clean water generation," *ACS applied materials & interfaces* **8**, 14628–14636 (2016).
15. H. Ghasemi, G. Ni, A. M. Marconnet, J. Loomis, S. Yerci, N. Miljkovic, and G. Chen, "Solar steam generation by heat localization," *Nat. communications* **5**, 4449 (2014).
16. G. Ni, S. H. Zandavi, S. M. Javid, S. V. Boriskina, T. A. Cooper, and G. Chen, "A salt-rejecting floating solar still for low-cost desalination," *Energy & Environ. Sci.* **11**, 1510–1519 (2018).
17. X. Li, W. Xu, M. Tang, L. Zhou, B. Zhu, S. Zhu, and J. Zhu, "Graphene oxide-based efficient and scalable solar desalination under one sun with a confined 2d water path," *Proc. Natl. Acad. Sci.* **113**, 13953–13958 (2016).
18. Y. Liu, S. Yu, R. Feng, A. Bernard, Y. Liu, Y. Zhang, H. Duan, W. Shang, P. Tao, C. Song *et al.*, "A bioinspired, reusable, paper-based system for high-performance large-scale evaporation," *Adv. Mater.* **27**, 2768–2774 (2015).
19. K. Kim, S. Yu, C. An, S.-W. Kim, and J.-H. Jang, "Mesoporous three-dimensional graphene networks for highly efficient solar desalination under 1 sun illumination," *ACS applied materials & interfaces* **10**, 15602–15608 (2018).
20. Q. Jiang and S. Singamaneni, "Water from wood: Pouring through pores," *Joule* **1**, 429–430 (2017).
21. C. Chen, Y. Li, J. Song, Z. Yang, Y. Kuang, E. Hitz, C. Jia, A. Gong, F. Jiang, J. Zhu *et al.*, "Highly flexible and efficient solar steam generation device," *Adv. materials* **29**, 1701756 (2017).
22. Z. Zhang, P. Mu, J. He, Z. Zhu, H. Sun, H. Wei, W. Liang, and A. Li, "Facile and scalable fabrication of surface-modified sponge for efficient solar steam generation," *ChemSusChem* **12**, 426–433 (2019).
23. Y. Wang, L. Zhang, and P. Wang, "Self-floating carbon nanotube membrane on macroporous silica substrate for highly efficient solar-driven interfacial water evaporation," *ACS Sustain. Chem. & Eng.* **4**, 1223–1230 (2016).
24. Q. Jiang, L. Tian, K.-K. Liu, S. Tadepalli, R. Raliya, P. Biswas, R. R. Naik, and S. Singamaneni, "Bilayered biofoam for highly efficient solar steam generation," *Adv. Mater.* **28**, 9400–9407 (2016).
25. G. Ni, G. Li, S. V. Boriskina, H. Li, W. Yang, T. Zhang, and G. Chen, "Steam generation under one sun enabled by a floating structure with thermal concentration," *Nat. Energy* **1**, 16126 (2016).
26. X. Li, R. Lin, G. Ni, N. Xu, X. Hu, B. Zhu, G. Lv, J. Li, S. Zhu, and J. Zhu, "Three-dimensional artificial transpiration for efficient solar waste-water treatment," *Natl. Sci. Rev.* **5**, 70–77 (2017).
27. N. Xu, X. Hu, W. Xu, X. Li, L. Zhou, S. Zhu, and J. Zhu, "Mushrooms as efficient solar steam-generation devices," *Adv. Mater.* **29**, 1606762 (2017).
28. Y. Liu, Z. Liu, Q. Huang, X. Liang, X. Zhou, H. Fu, Q. Wu, J. Zhang, and W. Xie, "A high-absorption and self-driven salt-resistant black gold nanoparticle-deposited sponge for highly efficient, salt-free, and long-term durable solar desalination," *J. Mater. Chem. A* **7**, 2581–2588 (2019).
29. H. Liu, X. Zhang, Z. Hong, Z. Pu, Q. Yao, J. Shi, G. Yang, B. Mi, B. Yang, X. Liu *et al.*, "A bioinspired capillary-driven pump for solar vapor generation," *Nano Energy* **42**, 115–121 (2017).
30. L. Zhu, M. Gao, C. K. N. Peh, and G. W. Ho, "Solar-driven photothermal nanostructured materials designs and prerequisites for evaporation and catalysis applications," *Mater. Horizons* **5**, 323–343 (2018).
31. M. Gao, L. Zhu, C. K. N. Peh, and G. W. Ho, "Solar absorber material and system designs for photothermal water vaporization towards clean water and energy production," *Energy & Environ. Sci.* **12**, 841–864 (2019).
32. X. Hu, W. Xu, L. Zhou, Y. Tan, Y. Wang, S. Zhu, and J. Zhu, "Tailoring graphene oxide-based aerogels for efficient

- solar steam generation under one sun,” *Adv. materials* **29**, 1604031 (2017).
33. J. Zhou, Z. Sun, M. Chen, J. Wang, W. Qiao, D. Long, and L. Ling, “Macroscopic and mechanically robust hollow carbon spheres with superior oil adsorption and light-to-heat evaporation properties,” *Adv. Funct. Mater.* **26**, 5368–5375 (2016).
  34. M. L. Brongersma, N. J. Halas, and P. Nordlander, “Plasmon-induced hot carrier science and technology,” *Nat. nanotechnology* **10**, 25 (2015).
  35. H. H. Richardson, M. T. Carlson, P. J. Tandler, P. Hernandez, and A. O. Govorov, “Experimental and theoretical studies of light-to-heat conversion and collective heating effects in metal nanoparticle solutions,” *Nano letters* **9**, 1139–1146 (2009).
  36. G. Liu, J. Xu, and K. Wang, “Solar water evaporation by black photothermal sheets,” *Nano Energy* **41**, 269–284 (2017).
  37. L. Zhou, Y. Tan, J. Wang, W. Xu, Y. Yuan, W. Cai, S. Zhu, and J. Zhu, “3d self-assembly of aluminium nanoparticles for plasmon-enhanced solar desalination,” *Nat. Photonics* **10**, 393 (2016).
  38. G. Zhu, J. Xu, W. Zhao, and F. Huang, “Constructing black titania with unique nanocage structure for solar desalination,” *ACS applied materials & interfaces* **8**, 31716–31721 (2016).
  39. M. Ye, J. Jia, Z. Wu, C. Qian, R. Chen, P. G. O’Brien, W. Sun, Y. Dong, and G. A. Ozin, “Synthesis of black tio<sub>2</sub> nanoparticles by mg reduction of tio<sub>2</sub> nanocrystals and their application for solar water evaporation,” *Adv. Energy Mater.* **7**, 1601811 (2017).
  40. J. Wang, Y. Li, L. Deng, N. Wei, Y. Weng, S. Dong, D. Qi, J. Qiu, X. Chen, and T. Wu, “High-performance photothermal conversion of narrow-bandgap ti<sub>2</sub>o<sub>3</sub> nanoparticles,” *Adv. Mater.* **29**, 1603730 (2017).
  41. D. Ding, W. Huang, C. Song, M. Yan, C. Guo, and S. Liu, “Non-stoichiometric moo 3- x quantum dots as a light-harvesting material for interfacial water evaporation,” *Chem. Commun.* **53**, 6744–6747 (2017).
  42. Y. Liu, J. Chen, D. Guo, M. Cao, and L. Jiang, “Floatable, self-cleaning, and carbon-black-based superhydrophobic gauze for the solar evaporation enhancement at the air–water interface,” *ACS applied materials & interfaces* **7**, 13645–13652 (2015).
  43. Y. Yang, R. Zhao, T. Zhang, K. Zhao, P. Xiao, Y. Ma, P. M. Ajayan, G. Shi, and Y. Chen, “Graphene-based standalone solar energy converter for water desalination and purification,” *ACS nano* **12**, 829–835 (2018).
  44. Y. Li, T. Gao, Z. Yang, C. Chen, W. Luo, J. Song, E. Hitz, C. Jia, Y. Zhou, B. Liu *et al.*, “3d-printed, all-in-one evaporator for high-efficiency solar steam generation under 1 sun illumination,” *Adv. materials* **29**, 1700981 (2017).
  45. X. Lin, J. Chen, Z. Yuan, M. Yang, G. Chen, D. Yu, M. Zhang, W. Hong, and X. Chen, “Integrative solar absorbers for highly efficient solar steam generation,” *J. Mater. Chem. A* **6**, 4642–4648 (2018).
  46. S. Loeb, C. Li, and J.-H. Kim, “Solar photothermal disinfection using broadband-light absorbing gold nanoparticles and carbon black,” *Environ. science & technology* **52**, 205–213 (2017).
  47. L. Zhou, S. Zhuang, C. He, Y. Tan, Z. Wang, and J. Zhu, “Self-assembled spectrum selective plasmonic absorbers with tunable bandwidth for solar energy conversion,” *Nano Energy* **32**, 195–200 (2017).
  48. C. Li, D. Jiang, B. Huo, M. Ding, C. Huang, D. Jia, H. Li, C.-Y. Liu, and J. Liu, “Scalable and robust bilayer polymer foams for highly efficient and stable solar desalination,” *Nano Energy* **60**, 841–849 (2019).
  49. A. H. Smith, P. A. Lopipero, M. N. Bates, and C. M. Steinmaus, “Arsenic epidemiology and drinking water standards,” (2002).